Available online at www.sciencedirect.com
SCIENCE DIRECT®
C. R. Mecanique 332 (2004) 767–781
COMPTES RENDUS MECANIQUE

Le Point sur.../Review Article

Various aspects of fluid vortices

Ivan Delbende [a,b], Thomas Gomez [b,c], Christophe Josserand [c,*], Caroline Nore [a,d], Maurice Rossi [c]

[a] *LIMSI-CNRS, BP 133, 91403 Orsay cedex, France*
[b] *Université Paris VI, 4, place Jussieu, 75252 Paris cedex 05, France*
[c] *LMM-CNRS, case 162, 4, place Jussieu, 75252 Paris cedex 05, France*
[d] *Université Paris XI, 91405 Orsay cedex, France*

Received 18 February 2004; accepted after revision 6 April 2004

Article written at the invitation of the Editors

Abstract

A general review of the current research in vortex dynamics is presented, based on contributions given during a workshop held in May 2003 at Porquerolles, France. This article aims at providing a picture of the work performed on this subject in the French community. Various cases are covered, from 2D vortex patches to 3D vortex tubes; from isolated vortices to shear flows. Different contexts are considered: pure Euler and Navier–Stokes flows as well as stratified, rotating and magnetic flows. ***To cite this article: I. Delbende et al., C. R. Mecanique 332 (2004).***

Résumé

Tourbillons en hydrodynamique. Nous présentons une revue des recherches actuellement menées dans le domaine de la dynamique des tourbillons. Elle s'appuie sur les travaux exposés lors de la conférence « Tourbillons en hydrodynamique » qui s'est tenue à Porquerolles en mai 2003. Les sujets abordés couvrent un large éventail thématique : du tourbillon bidimensionnel au tube de vorticité tridimensionnel, qu'il soit isolé ou au sein de couches cisaillées. Ces écoulements sont étudiés dans le cadre des équations d'Euler ou de Navier–Stokes et sont éventuellement soumis à des effets de stratification, de Coriolis ou de champ magnétique. ***Pour citer cet article : I. Delbende et al., C. R. Mecanique 332 (2004).***

Keywords: Fluid mechanics; Vortices; Shear flows; Geophysical flows; Magnetohydrodynamics; Control

Mots-clés : Mécanique des fluides ; Tourbillons ; Écoulements cisaillés ; Écoulements géophysiques ; Magnétohydrodynamique ; Contrôle

Porquerolles is an attractive little resort on the Levant Islands, well known for its delightful wines and noisy frogs. This southern most archipelago of the French Riviera was already noticed by the ancient greeks as the

* Corresponding author.
E-mail address: josseran@lmm.jussieu.fr (C. Josserand).

1631-0721/$ – see front matter
doi:10.1016/j.crme.2004.04.003

'Stoechades Islands'. It offered a perfect location for the conference held in May 2003 on various aspects of fluid vortices. From the large spectrum of fluid problems covered, it appeared that many flows can be approached in terms of the dynamics of an isolated vortex or several vortices. For instance, some aircraft wake properties can be understood in terms of the action of strain upon vortex wave propagation. This 'vortex approach' has been advantageously adopted in various domains, such as geophysics (atmospherical wakes, sand ripples), aeronautics (vortex breakdown, trailing vortices), and magnetohydrodynamics. In a more general setting, this point of view is also pertinent e.g. for shear flows (wakes, jets), turbulence problems (singularities in the Euler equation, vortex merging, strained fields) and control issues.

In this review article, we present an overall picture of the French contributions in this field, starting from basic concepts in 2D and 3D vortex flows, to more complex situations.

1. Pure two-dimensional vortices

Vortex dynamics can be considered to be two-dimensional whenever the flow shows a trivial behavior along one axis. Typical cases are geophysical, stratified and Hele–Shaw flows. Though pure 2D motions have peculiar topological constraints, their study is enlightening for a general understanding of fluid dynamics. Cascade processes in turbulent flows, mixing, boundary layer and Hamiltonian problems are typical examples where a 2D model is the first step toward a 3D theory.

A first theoretical viewpoint for 2D flows considers a system of point vortices. This approach presents important mathematical challenges as well as physical interest. For example, geophysical cyclones can be modelled using such a Hamiltonian dynamical approach on a sphere. Particular attention is given to cluster formation on a plane and a sphere. Simple cases with four vortices and given symmetries are analysed in [1]: by carefully studying the phase space, a bifurcation energy threshold is found to exist below which cluster formation occurs.

As far as turbulence is concerned, the Euler dynamics of point vortices does not include the merging process and therefore cannot offer a satisfactory model. Indeed, the turbulent flow behavior is constrained by two cascades. The inverse energy cascade, which follows a $k^{-5/3}$ law in momentum space, manifests itself in real space through vortex mergings, forming large-scale coherent structures. In addition, the direct enstrophy cascade towards small wavelengths is related to filamentary structures which are also present during merging. Following conservation rules, a dilute vortex gas model has been proposed [2] which phenomenologically includes the action of merging. Vortices interact like point vortices when they are far apart and fusion occurs when equal-sign vortices are close enough. Assuming that the vortex density decreases with time t as $t^{-\xi}$, scaling behaviors for the mean circulation and vortex radius are then deduced from this simple dynamics. This model is corroborated by numerical simulations which, in addition, provide the value of 0.75 for ξ. This latter value cannot be a priori determined by the heuristic model, since a careful understanding of the vortex merging dynamics is first needed.

Recent experiments have analyzed the merging of two co-rotating vortices in an almost pure 2D geometry [3]. Two identical vortices are generated in a water tank by an impulsive rotation of two plates. Different steps are identified during the fusion. First, the two vortices rotate around each other as point vortices and viscosity only intervenes by increasing the radius of each vortex core. When a critical ratio between the vortex radius and the distance between vortices is reached, a fast convective stage begins: the two vortices approach each other while vorticity filaments are ejected. This critical ratio for merging seems to correspond to the appearance of unstable modes in an equivalent Euler system. The full dynamics can be advantageously approached by direct numerical simulations (DNS) where streamlines are considered in the rotating frame of the co-rotating vortices [4]. An inner region around the vortices is identified and the velocity field can be thus separated in two components: one coming from the inner vorticity region, the other one from the outer region. The ejected vorticity is found to induce a velocity field that brings the two vortices closer, in agreement with experimental results [3]. This dynamics is self sustained since the decrease of vortex separation favors the transfer of vorticity into the filaments. Interestingly, for high Reynolds numbers, the vortex separation distance displays a plateau-like behavior before complete fusion

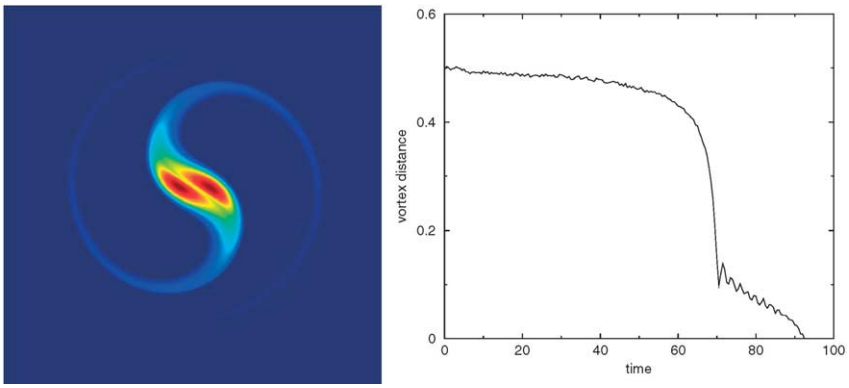

Fig. 1. Left: vorticity field during merging for $Re = 15\,000$ at time $t = 70$; right: vortex distance with respect to time.

is achieved (see Fig. 1). An important change in the streamfunction topology is also observed during this interval: the flow at the center of the system changes from a hyperbolic to an elliptic configuration. This third stage of the merging, recently observed in experiments, is called the second diffusive stage and viscosity is again important there.

In many experimental situations such as [3], vorticity is assumed to be marked by dye tracers. However dye is a passive scalar following an advection–diffusion equation. In 2D this is only an approximation for the vorticity evolution. Simultaneous numerical studies of vorticity and passive scalar distributions in turbulent flows are able to differentiate between the two cases [5]. More precisely, the conditional probability laws for second-order Lagrangian derivative of vorticity and passive scalar gradients are computed for both elliptic and hyperbolic regions of turbulent flows. It is observed that the numerical vorticity gradients present faster temporal fluctuations than passive scalar gradients. This property is conserved even when random velocity fields are considered.

2. Geophysical vortices

Large-scale vortices play an essential role in the dynamics of oceans and the atmosphere. In these stratified and rotating geophysical flows, the large-scale structures produced by shear instabilities are generally 2D due to strong effects of Coriolis and buoyancy forces that inhibit vertical motions. For instance, the wind flowing around mountain islands, revealed by the cloud patterns, generates a vortex street reminiscent of the classical Bénard–von Kármán street. However some geophysical wakes display a selective destabilization of cyclonic or anticyclonic vortices.

The geophysical flow dynamics is mainly characterized by two length scales: D the obstacle size and $R_d = \sqrt{gh}/2\Omega_0$ the deformation radius where g is the gravity, h the fluid depth and Ω_0 the Earth rotation. Three dimensionless parameters are relevant: the Burger number $Bu = (2R_d/D)^2$ (ratio of the gravity and rotation effects), the Reynolds number $Re = UD/\nu$ (U is the velocity scale and ν the kinematic viscosity) and the Rossby number $Ro = U/D\Omega_0$ (ratio of the advective and Coriolis terms).

Large-scale geophysical wakes ($D \gg R_d$ or equivalently $Bu \ll 1$) can be studied in the rotating shallow-water context. This situation is approached by a rotating two-layer experiment as well as numerical simulations. Experimentally, a thin fresh-water layer lies on a thick salt-water layer. The presence of the bottom layer is only here to ensure that the interface between the fresh- and salt-water behaves like a free-surface. A vortex street is created by towing an obstacle within the upper layer. As the Burger number increases from $Bu = 0.1$ to 1, the asymmetry between cyclonic and anticyclonic vortices is enhanced: the cyclones become more elliptic whereas the anticyclones remain axisymmetric. Numerical simulations combining a pseudo-spectral scheme with a volume

penalization method to take the obstacle into account are in good agreement with the previous experiments near Reynolds number $Re = 400$ and Rossby number $Ro = 0.25$ [6].

In order to investigate a large Burger number ($Bu \gg 1$) situation, another experimental setup has been devised: an elongated cylinder is pulled in a rotating tank to produce the geophysical Bénard–von Kármán street. At intermediate Reynolds numbers ($Re \approx 150$), order one Rossby numbers ($Ro \approx 0.4$–4) and large Burger numbers ($Bu \approx 10^3$–10^4), the previously reported asymmetry is reversed between cyclones and anticyclones. Cyclones are found stable and axisymmetric whereas anticyclones characterized by a weak elliptic distribution of vorticity become unstable. This destabilization occurs in the vortex core as in the elliptic instability while the vortex periphery remains unaffected. Moreover, unlike the centrifugal instability, the vertical wavelength increases with the Rossby number Ro [7]. Therefore this asymmetry is probably due to the inertial elliptic instability rather than to the centrifugal instability.

Vortices can also be observed at very different geophysical scales e.g. during the formation of sand ripples on a beach. This process has been mimicked in an annular tank filled with a sand layer on top of which an upper layer of fluid oscillates. An initial pattern emerges consisting of small amplitude and wavelength 'rolling grain ripples'. PIV measurements described in [8] show that a vortex is shed from each of the crests in alternate directions during each half period. These new observations contradict the usually inferred mechanism for crest formation based on the presence of two counter-rotating vortices between two successive crests. However, this initial pattern eventually gives way to the formation of large amplitude and wavelength 'vortex ripples'.

3. Pure three-dimensional vortices

Vortices are classically known to sustain propagating waves called Kelvin or inertial waves. Most features pertaining to the vortex three-dimensional dynamics depend on the phase and group velocities as well as on the spatial structure of these waves. Such aspects have been studied [9] on a typical smooth vorticity profile: the Lamb–Oseen vortex $V_\theta = \Gamma(1 - \exp(-(r/a)^2))/2\pi r$ where Γ, a denote the circulation and vortex core size, respectively. In the remaining part of this section we use dimensionless quantities based on Γ and a. A viscous stability analysis in terms of normal modes $f(r)\exp(\mathrm{i}kz + \mathrm{i}m\theta - \mathrm{i}\omega t)$ with $\omega \equiv \omega_r + \mathrm{i}\omega_i$ confirms that all modes (k, m) are stable ($\omega_i < 0$). If the axisymmetric modes ($m = 0$) are weakly affected by viscosity, this is not the case of double helix modes $|m| = 2$ and higher modes $|m| > 2$, which generally undergo a significant damping. The influence of the Reynolds number $Re \equiv \Gamma/2\pi\nu$ on helical modes ($m = \pm 1$) is quite dependent on ω_r/m the angular velocity in the vortex cross-section. For left-handed helical waves ($k/m > 0$), the following trends are observed. Modes with $\omega_r/m > 1$ propagate along the vortex in the positive axial direction and are particularly damped for long axial wavelength $k \to 0$ where their spatial structure becomes concentrated near $r = 0$. Helical modes with $0 < \omega_r/m < 1$ are singular (critical layer) and highly damped. Finally modes with $\omega_r/m < 0$ propagate along the vortex in the negative axial direction. Among these, the so-called bending or slow mode corresponds to the translation of the vortex axis without modification of its internal structure. This mode, which is characterized by a group velocity tending towards zero for $k \to 0$, is barely modified by viscosity. Right-handed waves ($k/m < 0$) have similar properties and opposite group velocities. An initial value simulation for $Re = 1000$ confirms the above features by displaying the response of a Lamb–Oseen vortex to an initially localized left-handed perturbation after several overturn periods. Because of its negative group velocity and its small damping, the slow wave mode rapidly emerges from a localized perturbation. A fraction of the energy, concentrated in the singular modes, does not propagate and is rapidly damped. Another small fraction is contained in a concentrated structure propagating in the positive direction.

The transient evolution of perturbations superimposed to the Lamb–Oseen vortex can be characterized by another approach [10]. Instead of resorting to standard normal modes analysis, one uses the so-called non-normal approach based on an optimization problem: given a perturbation of the form $f(r,t)\exp(\mathrm{i}kz + \mathrm{i}m\theta)$, find the optimized time τ corresponding to a maximum amplification gain $G(\tau) = E(\tau)/E(0)$ of the disturbance kinetic

energy $E(t)$. Given the parameters (k, m) and Reynolds number *Re*, this optimization problem is solved by an iterative procedure. The curve of maximum amplification versus axial wavenumber k for modes $m = 1$ possesses a peak at a short wavelength $k \approx 1.4$ which is almost independent of the Reynolds number. However the maximum amplification $G(\tau)$ and the optimized time τ corresponding to these wavenumbers (k, m) evolve with *Re* leading to significant growth even at moderate *Re*. The initial optimal perturbation can be described as spiral sheets subsequently evolving at the optimized time τ into a strong bending wave in the vortex core. This evolution is reminiscent of the Orr mechanism active in boundary layers.

4. Three-dimensional vortices in the presence of a strain field

The previous section addresses the dynamics of perturbations propagating on a given vortex profile assuming that the action of other vortices and boundaries can been disregarded. However, a closer look at this dynamics under the influence of external factors may be necessary. This is true for the problem of four vortices in a counter-rotating configuration. Such a seemingly 'baroque' configuration appears commonly in aircraft wakes during landing or take-off and is known to have time dependent i.e. periodic, stationary or divergent solutions. It is interesting to analyze its stability in order to promote the disruption of this configuration in real cases. The problem has been studied [11] using an analogue to the linearized vortex filament method developed for the Crow instability of two counter-rotating vortices. The long wavelength approximation provides a non-autonomous eighth-order dynamical system which describes the mean positions of the four vortices. The non-normal technique mentioned in the previous section is then employed for this time dependent problem since it by-passes the assumption of an exponentially growing normal mode. The results indicate that the weak Crow instability of the stronger vortices, i.e. the aircraft outboard vortices, can be enhanced by the presence of a second vortex pair, i.e. the aircraft inboard vortices. The optimal amplifications are obtained for unrealistic aircraft engineering conditions. However, some net amplification is clearly possible for realistic situations: the Crow instability may thus be controlled by manipulating the other vortex pair. Nevertheless such encouraging results may be modified in the nonlinear regime.

The potential flow due to other vortices or boundaries may also lead to profound modification of the internal dynamics of a given vortex. Inside the vortex, an external strain may be approximated under the strain $(\alpha x, \beta y, \gamma z)$ where z denotes the vortex axis. If the strain is purely 2D ($\alpha = -\beta$ and $\gamma = 0$), the basic vortex streamlines deform and become elliptic. This effect leads to a generic core mechanism: the elliptic instability. This aspect has been experimentally explored [12] using a deformable shell filled with water which is rotated at constant angular speed while two or three rollers are positioned at the periphery so that a dipolar or tripolar excitation is applied to the flow. This set-up generates a columnar vortex submitted to a dipolar or tripolar strain. Instability modes arise from the resonance of two vortex Kelvin waves caused by the presence of the external strain. When the aspect ratio and the number of rollers are varied, several modes have been observed due to resonances between azimuthal wavenumbers ($m = -1$, $m = 1$), ($m = 0$, $m = 2$), ($m = 1$, $m = 3$). For the triangular forcing, resonance modes were found for the pairs ($m = -1$, $m = 2$) and ($m = 0$, $m = 3$). With increasing Reynolds number, such modes first undergo a nonlinear saturation towards a stationary state, then sustain a secondary instability, and eventually reach a stage where the vortex structure breaks down into small scales. The explosion is thereafter followed by a relaminarization of the flow, generating a new elliptical or tripolar vortex and thus a new instability cycle. These observations are in close agreement with a weakly nonlinear analysis though the explosion is clearly still to be elucidated. More recently another geometrical configuration has been considered, namely a sphere [13]. A spin-over mode is evidenced whereby an S-shaped vortex gradually tilts and saturates nonlinearly. Intermittent behavior has also been observed in this experiment. This new set-up is of great interest since it is an experimental analogue of the earth's liquid iron core subjected to tidal deformations. The question is raised whether this phenomenon has a link with the earth's magnetic field reversals and more generally with the dynamo problem.

Another possible strain corresponds to the three-dimensional axisymmetric case $\gamma/2 = -\alpha = -\beta > 0$ e.g. the celebrated Burgers vortex. Strangely enough, the stability of this classical Navier–Stokes solution had not been

considered. In [14], the Burgers vortex is shown to be asymptotically stable to any three-dimensional perturbations though significant transient growth may be present. This result is obtained by using an extended spatio-temporal Lundgren transformation and a time-dependent non-dimensionalization, which reduce this problem to the linear stability of the Lamb–Oseen vortex up to a time-dependent factor affecting the axial gradient terms. The transformed problem can then be solved by an optimization problem. A spatio-temporal Lundgren's transformation was also used to detect solutions which possess a finite time singularity in the context of the Euler or Navier–Stokes equations. This singularity which may stand at the heart of the turbulence problem has been observed in numerical simulations. In order to avoid the possible numerical origin of such a divergence, another viewpoint has been adopted [15]: a change of space–time variables is used to transform the singular behavior in the Euler equations into regular behavior of a transformed Euler problem. Introducing the new time variable $\lambda = -\log([t^* - t]/t^*)$, the Euler equations can be transformed into a system of equations which are autonomous in the logarithm of time, in such a way that the time of the hypothetical singularity t^* is sent to infinity. The form of the transformed velocity U is dictated by the conservation of circulation: $u(r, z, t) = \sqrt{\Gamma/(t^* - t)}\, U(R, z)$ where R denotes the transformed length $R = r/\sqrt{\Gamma(t^* - t)}$. It is argued that for an axisymmetric flow with swirl, the constraints arising from the conservation of energy and circulation are compatible with a solution collapsing on a line [16]. Leaving the axial space variable unaffected by the similarity transformation, it is shown that the problem can be reformulated in terms of a streamfunction and a circulation variable, following the Bragg–Hawthorne procedure. This leads a set of explicit equations. If such equations possess a smooth solution satisfying certain conditions, the original Euler equations then possess a finite-time singularity.

Going back to experimental considerations, the Burgers vortex profile is difficult to isolate in an experimental situation similarly to what was achieved for the elliptic instability [12]. In [17], a stretched vortex is generated in a water channel. A boundary layer first develops due to an inflow of mass flux Q_1. The separation, roll-up and suction of this boundary layer then generates a vortex which is symmetrically attached to two holes located at each side wall. The flux Q_2 entering these two openings equals the entire mass flux Q_1. The vortex velocity field is much more involved than a pure Burgers vortex since the axial stretching $\partial_z V_z$ varies along the vortex axis as well as along the radial direction. Note that the vortex core is much smaller than the size of the holes. An asymptotic analysis coupled to a closure assumption has led to a theoretical model which nicely fits the PIV measurements obtained in the water channel. Experiments have also been conducted so as to characterize the dynamics of this basic stretched vortex or of the waves it may support. For instance, the power dissipated due to the axial gradient has been measured to be of the same order as the power dissipated due to the azimuthal velocity.

When the mass flux Q_1 is not completely sucked into the two holes, the vortex can be bent (Q_1 larger but close to Q_2) or an almost periodic cycle of vortex creation and destruction appears (Q_1 larger than a critical value proportional to $Q_2^{2/3}$) [18]. This latter case is characterized by the generation of the vortex, its downstream motion followed by its detachment from the two holes and an abrupt breakdown the underlying mechanism of which is not fully understood. This burst generates small scales. From a velocity signal $u(t)$ measured around the explosion location during a long enough period (two thirds of the rotation period), one can find a $k^{-5/3}$ energy spectrum. This experimental result can be associated with the numerical procedure followed by Lundgren. Another experiment [19] has been deviced to generate a stretched vortex. Two co-rotating disks generate a background vorticity while suction is applied through the hole located at the center of each symmetric disk. This motion produces a symmetric stretching which concentrates the Ekman vorticity and creates a vortex filament. The pressure gradient which is imposed to get a constant mass flux through the holes has been shown to depend on the vortex: for low disk rotation, the pressure increases with rotation due to a pure stretching effect. For higher rotation, the vortex is strong enough and counterbalances this effect by a centrifugal effect in the vortex center leading to a decrease of the pressure gradient with rotation.

5. Three-dimensional vortices in the presence of an axial jet

In fully turbulent flows as well as in aircraft wakes, coherent vortices may sustain an axial jet component which alters considerably their stability properties. The prototype of such trailing vortices – also an asymptotic solution – is the Batchelor vortex, also known as the q-vortex:

$$V_r(r) = 0, \qquad V_\theta(r) = \frac{\Gamma}{2\pi a}\,\frac{1-\mathrm{e}^{-(r/a)^2}}{r/a}, \qquad V_z(r) = W\,\mathrm{e}^{-(r/a)^2},$$

where Γ denotes the circulation and a the core size, identical for both jet and swirling components. The Reynolds number $Re = Wa/\nu$ is based on the maximum axial velocity W. The inviscid stability of this flow is governed by the swirl number $q = \Gamma/(2\pi aW)$: the trailing vortex becomes inviscidly unstable below a critical value $q_c \approx 1.5$ with respect to helical perturbations with azimuthal wavenumber $m < 0$.

While inviscid instabilities are well documented, the systematic investigation of viscous instabilities is quite recent [20]. It has been shown that viscous instabilities are likely to grow at any swirl level as $Re \to \infty$ (which is a singular limit). More precisely, the critical swirl level above which the flow is stable is shown to behave asymptotically as $q_c \approx 0.14Re^{1/3}$, the critical mode being $m = -1$. The structure of the modes prevailing at high swirl consists of viscous oscillations localized around the vortex centerline (for radial distance $r < Re^{-1/6}$). They can be analyzed in analogy with the wavefunction of a quantum particle in a semi-infinite potential sink [21]. Located in the core, these modes should exist for any trailing vortex, and might be linked with vortex meandering, a well-known phenomenon in aerodynamics, which is still unexplained. At low swirl level, other viscous modes prevail: 'ring modes' which can be studied in analogy with the quantum double-infinite sink problem. Even though the associated growth rates are rather small, these findings considerably widen the rather confined instability domain predicted in the inviscid frame.

When two trailing line vortices are present as in the far wake of an aircraft, the mutual effect consists, besides the downwards pair translation, of an elliptic deformation of the structures. In pure vortices, i.e. without axial flow, this effect is known to enhance the elliptic instability with maximum dimensional growth rate $\sigma = \frac{9}{16}\gamma$. This effect has been examined in the case where an axial flow is superimposed on the vortex [22]. For the Rankine vortex with top-hat jet profile, the elliptical instability persists. In contrast, when the vorticity is not localized in space as e.g. in the Batchelor vortex, the mode structure involves critical layers which are thought to dampen the elliptical instability. Other resonance modes might arise.

Axial strain applied to a Batchelor vortex flow is likely to enhance instability [22]. More specifically, axial compression preserves the axisymmetry of the flow which remains a Batchelor vortex, but it is able to lower the instantaneous swirl number $q(t)$ below its critical value at 1.5. For sufficiently small strain rates $\gamma \ll 1$, the instantaneous growth rate is shown to be related to the growth rate of an unstretched flow *via* a quasi-static approximation. The predicted growth of inviscid helical instabilities has been corroborated by DNS of the Navier–Stokes equations using Lundgren variables, linearized in the vicinity of the compressed/stretched Batchelor vortex at $Re \approx 670$, showing the effective growth of interwoven filaments (see Fig. 2). These findings have been proposed as a simple mechanism to explain the sudden burst of intense vortex structures as observed in fully turbulent flows. Assuming that the large-scale motion acts as a strain field on the vortex, it could lead to the disruption of initially stable vortices with high initial swirl level.

When one is interested with the long-time behavior of trailing vortices, it is natural to investigate the nonlinear dynamics of the primary instability. A range of swirl numbers is particularly interesting: when $1 \lesssim q \lesssim 1.5$, the vortex destabilizes through the inviscid instability mechanism, but nonlinear effects eventually lead to restabilization due to a decrease of the mean axial flow, thus an effective increase of swirl above the critical value 1.5. In [23], this latter property has been interpreted in the framework of local instability with respect to radial distance r in the short-wave limit. More precisely, a buffer zone has been shown to exist when $q \gtrsim 1$ at the periphery of the vortex, where the Leibovich–Stewartson criterion, a necessary condition for stability in trailing vortices, is locally satisfied. By DNS of the full Navier–Stokes equations at $Re \approx 3120$, it has been shown how

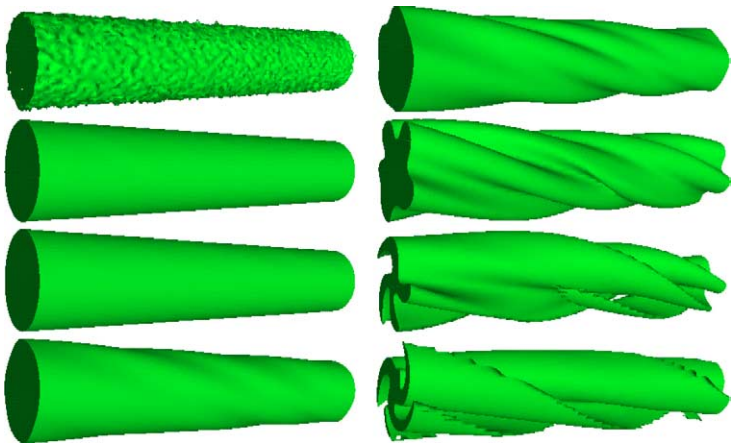

Fig. 2. Time evolution of a initially stable Batchelor vortex when submitted to time varying strain at $Re = 670$ (half-period of axial compression followed by half-period of axial stretching).

the turbulence initiated in the core region takes energy preferentially from the axial flow component and is then dispersed through the buffer zone as inertial waves, without any pumping of azimuthal velocity. This induces a swirl rate increase and a restabilization of the turbulent core, features to which the persistence of trailing vortices in aircraft wakes is ascribed.

6. Three-dimensional vortices in the presence of stratification

In stratified flows encountered in geophysical contexts, a major question which is still unanswered concerns the relationship and difference between a pure two-dimensional turbulence and geophysical turbulence in which motions are almost quasi-horizontal due to the strong influence of stable density stratification or Earth rotation.

Numerical simulations reveal the presence of a horizontally layered structure in stratified flows, which enhances energy dissipation. In addition, large scale structures have always a limited vertical extent like 'pancakes' and layers appear to be decoupled. An instability mechanism may be responsible for this decoupling. Such an assumption has been tested in the simpler context of the relaxation of a pair of long co- or counter-rotating vertical columnar vortices in a stratified fluid. When the vortices are counter-rotating, the Crow instability (see Section 4) and the short scale elliptic instability are inhibited by stratification. However, a third instability called zigzag instability arises. This process which can be interpreted in terms of slow bending Kelvin modes, slices the columnar vortex pair into horizontal layers of pancake-like dipoles [24–26]. A typical wavelength scales like U/N, where U is the horizontal velocity scale and $N = \sqrt{g\partial_z \rho/\rho}$ the Brunt–Väisälä frequency. An equivalent experimental situation has been studied in a tank filled with a linearly stratified salt solution in which a columnar vertical pair of vortices is created by rotating two flaps. This flow is characterized by two dimensionless parameters: the horizontal Froude number $F_h = U/NR$ (ratio of buoyancy and inertial forces) and the Reynolds number $Re = UR/\nu$ where U, R and ν are the initial propagating speed, the dipole radius and the mean kinematic viscosity, respectively.

When the two vortices are corotating, numerical and theoretical studies show for a large range of Reynolds numbers ($Re \approx 100$–$15\,000$) the existence of two kinds of instabilities [27]. For weak stratification ($F_h \gg 2$), the dominant instability is of the elliptic type with two unstable modes. For strong stratification ($F_h < 2$), a zig–zag-like phase instability occurs instead, involving a single unstable symmetric mode.

Another experiment has been carried on a counter-rotating pair of vortices in a stratified fluid, placed on a rotating platform. Two other types of instabilities have been observed solely affecting the anticyclonic vortex: an

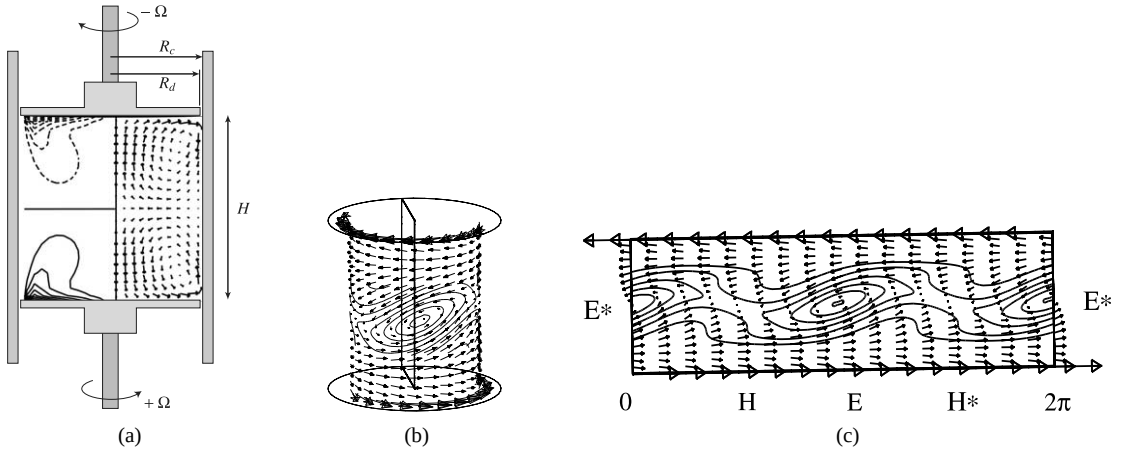

Fig. 3. (a) Experimental configuration. The inset illustrates azimuthal velocity contours (left) and meridional velocity field (right) of the axisymmetric flow determined by numerical simulation [30]. (b) Velocity field and radial vorticity at a fixed radius showing a steady corotating pair of vortices. (c) Unrolled quantities as in (b).

axisymmetric centrifugal mode and a new asymmetric oscillatory mode. A stability analysis of the Lamb–Oseen vortex indicates that the mechanism for the asymmetric instability is centrifugal.

7. Shear layers and sheets

7.1. Vortices in shear layers

The famous inviscid Rayleigh criterion states a necessary instability condition: an unstable 2D profile $u(y)\mathbf{e}_x$ must present an inflexion point. In mixing layers this instability is called the Kelvin–Helmholtz instability. Such a mechanism is characterized by a vorticity field $\omega_z(y)\,\mathrm{e}^{\mathrm{i}\alpha x}\mathbf{e}_z$ and gives rise to a chain of co-rotating cat's eye vortices. The flow driven by two counter-rotating disks displays vorticity patterns bearing a resemblance to the above mentioned vortices. This has been shown in two recent studies where the geometries of the forcing system are different: in [28], the flow is produced by the counter-rotation of the bottom disk and the top disk attached to the lateral wall; in [29,30], the lateral wall is fixed (see Fig. 3). The common non-dimensional parameters are the height-to-radius aspect ratio $\Gamma = H/R$ and the ratio of the angular disk velocities $s = \Omega_{\mathrm{top}}/\Omega_{\mathrm{bot}}$. The resulting pattern in [28] is a superposition of vertical co-rotating vortices connected to the boundary layers through spiral arms. Experimental and numerical results performed for various s and small values of Γ collapse on the same instability curve for spirals and vortices. This proves that such structures are two aspects of the same instability due to the following mechanism: the centrifugal effects of each rotating disk create a detached boundary layer over the slower disk, leading to a free shear layer of velocity $u_\theta(r,z)\mathbf{e}_\theta$ in the bulk of the flow. Treating the z-dependence as parametric, the basic profile $u_\theta(r)$ can give rise to vertical Kelvin–Helmholtz vortices. In contrast, the resulting pattern in [29] where the two disks are exactly counter-rotating is a chain of radial co-rotating vortices. For different $\Gamma = \mathrm{O}(1)$, the basic state is unstable through the Kelvin–Helmholtz instability of the equatorial azimuthal shear layer created between the two recirculating zones due to Ekman pumping. The analysis is performed using a basic velocity profile $u_\theta(z)$ neglecting the r-dependence. The results are compatible with the emergence of radial vortices at the Kelvin–Helmholtz threshold. In these examples, the instability of the free shear layer $u_\theta(r,z)$ gives rise to vortices of different orientations depending on the geometry of the forcing.

The above analysis is based on simplified basic profiles where stretching and curvature are neglected. By contrast, the effect of an external hyperbolic strain flow is introduced in [31,32] for the Kelvin–Helmholtz

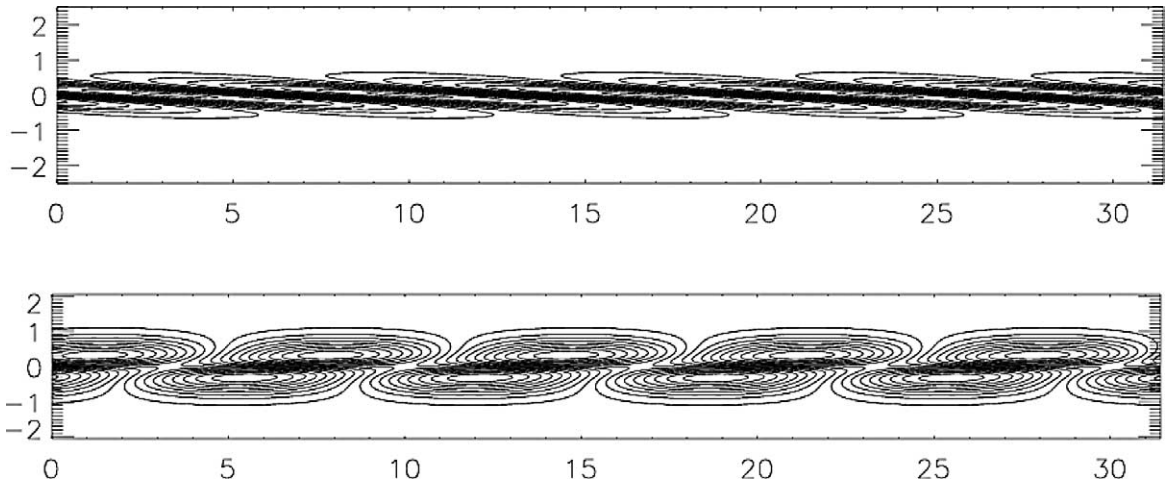

Fig. 4. Vorticity isocontours of the most amplified perturbation at $t = 20$ for a stretched shear layer. Top: at $t = 0$; bottom: at $t = 20$.

instability in the context of inviscid and viscous dynamics. Due to stretching, the basic flow $u(y,t)\mathbf{e}_x$ is now unsteady. The evolution of perturbations is to be studied in the non-normal analysis framework in order to obtain the maximum amplification gain at a given time. The inviscid study is performed on a basic broken-line velocity profile perturbed by 2D unsteady disturbances defined by a streamfunction $\phi(y,t)\,\mathrm{e}^{\mathrm{i}kx}$. A negative stretching (compressive zone) stabilizes the mixing layer while a positive stretching is destabilizing. In the viscous limit, the basic state is chosen to be the standard $\tanh(y/\delta(t))$ profile with a time-varying width $\delta(t)$ due to the unsteady stretching. Evaluation of the maximum amplification gain of perturbations is performed using the adjoint operator. This viscous approach demonstrates that the main conclusions of the inviscid case are not affected. A view of the disturbance which is optimal at $t = 20$, is shown at $t = 0$ and $t = 20$ in Fig. 4.

Two classical flows evade the inflexion point criterion and present a strong analogy: Taylor–Couette (TC) and plane Couette (PC) flows. Both are produced by the differential motion of their boundaries: differential rotation of the two co-axial cylinders in TC, differential translation of the two plates in PC. A recent research axis has taken advantage of the analogy between the two flows: known patterns in TC such as rolls and banded turbulence have been demonstrated in PC, both experimentally and numerically. In PC, the dynamics is governed by one non-dimensional parameter, the Reynolds number $Re \equiv \Delta u \Delta y/\nu$ where $2\Delta u$ denotes the differential translation velocity and $2\Delta y$ the spanwise distance between the two plates. In TC, there are three dimensionless parameters: the aspect ratio $\eta \equiv r_{\mathrm{in}}/r_{\mathrm{out}}$, the ratio of angular velocities $\mu \equiv \Omega_{\mathrm{out}}/\Omega_{\mathrm{in}}$ and the Reynolds number $Re \equiv r_{\mathrm{in}}\Omega_{\mathrm{in}}d/\nu$ where r_{in} and Ω_{in} (resp. r_{out} and Ω_{out}) are the inner (resp. outer) radius and angular velocity. $2d$ is the gapwidth. In [33,34], the PC flow perturbed by a thin spanwise-oriented ribbon shows a first bifurcation towards 3D streamwise rolls at $Re \simeq 230$. This bifurcation is followed by various others towards a series of stable and unstable steady states presenting different wavenumbers and symmetries. However transition to turbulence occurs around a higher Reynolds number ($Re \simeq 300$) and is as sudden and unexplained as that occurring in PC flows without ribbon. Hence, there is apparently no connection between the low-Reynolds number bifurcations of the ribbon-perturbed PC and the transition to turbulence in the classical PC flow. In [35], transient growth is studied in counter-rotating TC flows as a function of aspect ratio η and Reynolds number Re. The PC case is recovered for $\eta = 1$. For $Re \leqslant 500$, the greatest transient amplification is achieved for a value of $\eta < 1$, meaning that transient growth is enhanced by curvature. The optimal inputs are concentrated in the meridional velocity components while the optimal outputs are dominated by the azimuthal velocity component. This modification is due to the creation of streaks by the vortices which is also the essential mechanism for the transition to turbulence in PC flow.

7.2. Vortex sheet roll-up

Vortex sheets can be numerically studied using Lagrangian vortex methods: vorticity is represented as a collection of N vortex points and the evolution is governed by a system of N ordinary differential equations. The induced Lagrangian velocity $\mathbf{U}_p$ of a particle p situated at $\mathbf{r}_p$ is given by the Biot–Savart law: $\mathbf{U}_p = \sum_{q=1}^{N} \mathbf{K}(\mathbf{r}_q - \mathbf{r}_p, \delta) \wedge \boldsymbol{\Omega}_q$ where $\boldsymbol{\Omega}_q$ is the vector vorticity weight. The Green kernel for the vector Laplacian operator $\mathbf{K}_{2D}(\mathbf{r}) = -\mathbf{r}/2\pi r^2$ or $\mathbf{K}_{3D}(\mathbf{r}) = -\mathbf{r}/4\pi r^3$ must be regularized so that the $r = 0$ singularity is smoothed. A small regularization parameter δ is thus introduced: in the 2D study [36], the kernel $\mathbf{K}(\mathbf{r}, \delta) = -\mathbf{r}/2\pi(r^2 + \delta^2)$ is used, while in the 3D study [37], $\mathbf{K}(\mathbf{r}, \delta) = -\mathbf{r}/4\pi\sqrt{r^6 + \delta^6}$.

In [36], an initially unstable vortex sheet discretized as a line of point vortices is considered. The vortex sheet develops a Kelvin–Helmholtz instability. During its nonlinear time evolution, a perturbation is added to test the sensitivity of the sheet against a secondary instability. The evolution of this perturbation towards secondary vortices depends on the local strain rate: stretching inhibits growth while compression enhances it.[1] It is found that the growth rate and the characteristic length scale of the secondary instability are fixed by the regularization parameter δ. During the subsequent nonlinear time evolution, the stretching rate varies in time and space and is directly related to the density of vortex points along the sheet. This density is concentrated in peaks distributed along the sheet and gives rise to an intermittent distribution of vorticity. Such a phenomenon results in a k^{-4} velocity spectrum similar to that found in 2D turbulence.

The vortex method has been tested in 3D in the case where a circular jet is emitted into a medium with lateral flow [37] (like a chimney exhaust in the wind): a leading vortex ring forms and is eventually stretched. A 'remeshing' procedure is then necessary, whereby particules are redefined with new $\boldsymbol{\Omega}_q$ weights at the nodes of a regular mesh, in such a way that the physical properties of the flow are preserved. This procedure also prevents particles from becoming locally too dense or too sparse. The number of particles is controlled by an empirical vorticity threshold below which the particles are suppressed. This method qualitatively accounts for the dynamics of a jet bent by a lateral flow, including the formation of vortex rings and of two curved streamwise counter-rotating vortices.

8. Vortices in wakes

Cylinder wakes have often been considered as the archetype of wake flows, especially regarding the sequence of instabilities arising when the Reynolds number $Re = UD/\nu$ (D denotes the diameter) is gradually increased. Above the critical value $Re_c = 47$, the celebrated Bénard–von Kármán vortex street occurs. The alternate saturated primary vortices form a quasi-periodic pattern of streamwise wavelength λ_{2D}, which may then sustain secondary instabilities: when $Re > 190$ a three-dimensional symmetric (or A-) mode of spanwise wavelength $\lambda_A \approx \lambda_{2D}$ grows; for $Re > 260$ it is replaced by an anti-symmetric (or B-) mode of much smaller wavelength $\lambda_B \ll \lambda_{2D}$.

A thin flat plate wake [38] differs significantly from that of a cylinder: both types of modes can be observed at the same Reynolds number above threshold, and the wavelength λ_a of the anti-symmetric mode is about the same as that λ_s of the symmetric one ($\lambda_a \approx \lambda_s \approx \lambda_{2D}$). A temporal study of these secondary instabilities has been numerically performed [39]: one spatial period of the basic flow is first obtained by a 2D DNS of a Bickley wake (velocity deficit proportional to $\cosh^2(y/d)$) in the vicinity of which the 3D evolution Navier–Stokes operator is linearized. The maximum growth rates of the leading symmetric and anti-symmetric modes are found to be equivalent. They are attained at comparable wavenumbers. This supports the occurrence of both patterns for the same experimental conditions with about the same wavelength. The local elliptic instability theory applied at the

[1] This result seems to contradict the conclusions of [31,32]. The difference is due to the geometry: the stretching is 2D in [36] while it is 3D in [31,32].

elliptic point in the primary vortex cores (where the local strain rate is γ) allows one to evaluate a maximum growth rate $\sigma = \frac{9}{16}\gamma$ in very good agreement with the growth rates obtained numerically. By contrast, the local hyperbolic theory in the braid leads to growth rates up to 5 times larger, a feature which is never observed numerically. Hyperbolic regions can at most sustain intense transient growth, but their long time perturbation growth seems always slaved to that of the elliptic point.

Sphere wakes are very different from cylinder or plate wakes. For $210 < Re < Re_c = 280$, the flow behind a sphere consists of two stationary counter-rotating streamwise vortices. Above Re_c, vortex loops are shedded periodically. This now well-documented dynamics is relevant in bubbly or particle-laden flows for low concentrations. At higher concentrations, neighboring objects interact, as in the following experiment [40]. Two spheres are placed side by side in a uniform flow. When they are sufficiently spaced, their wakes are uncoupled. Several regimes are then observed as the spacing between the spheres is gradually reduced: in-phase oscillations, anti-phase oscillations, and eventually strong mechanical vortex-induced vibrations. In this latter case, a DNS shows that the inter-sphere flow sticks to one of the spheres, or to the other: the observed vibrations may be linked to this bi-stability property. For touching spheres, a single wake is obtained. Other experiments reveal the dynamics of the flow in the vicinity of a single sphere moved orthogonally towards a solid plane or a free-surface and abruptly stopped [41].

The backward-facing step constitutes a basic model of boundary layer separation since it contains a feature at the heart of any wake flow structure: a recirculation region. This situation is also present in many industrial problems. This flow has been investigated experimentally in the stationary regime [42]. The presence of a three-dimensional stationary structure periodic in the spanwise direction has been ascertained by PIV measurements. This pattern causes the recirculation length, which is proportional to Reynolds number, to vary along the span with a spatial period independent of the step height and of the Reynolds number. Moreover counter-rotating longitudinal vortices have been detected. The observed structures seem consistent with the presence of a Görtler instability due to the curvature of streamlines just downstream of the recirculation region.

A similar problem has been numerically investigated [43]: the boundary layer gets separated due to a bump mounted on a flat plate. The problem, however, is kept purely two-dimensional here and the work focuses on the stability of the recirculation region. Below a critical Reynolds number Re_c, the computed steady flow is convectively unstable. Above this Re_c, the flow undergoes an unsteady transition leading to a time periodic shedding of vortices downstream at low frequency. An analysis of the computational results indicates that such oscillations are due to a change of topology about to take place at the re-attachment region i.e. the breakup of the recirculation zone. It is inferred that this breakup may trigger an abrupt transition towards an absolute instability leading to self-sustained modes at low frequency. By adding a smaller bump behind the first one, it is possible to delay this transition by re-accelerating the boundary layer and to produce a true global mode transition with a clean periodic motion at a global frequency distinct from the previous low frequency and predicted by a nonlinear frequency criterion.

9. Vortices and control

At the end of the previous section, the flow has been manipulated by adding a small bump which affected the overall structure. This is a typical control strategy used to enhance or to reduce some features at the lowest possible cost. For instance, it is advantageous to reduce the longitudinal vortices produced by the edges of a road vehicle. Indeed such structures significantly change the vehicle drag coefficient. Such a control strategy can be for instance applied to the Bénard–von Kármán vortex street in a cylinder wake [44]. An experimental procedure has been actually attempted where the cylinder is made to rotate in an oscillatory manner with given frequency and amplitude. When the amplitude is high enough to lock in the shedding frequency to the forcing frequency, the vortex street is indeed suppressed and the drag is considerably reduced. However the oscillation amplitude is still large.

The vortex breakdown phenomenon is another hydrodynamic aspect which could be also tentatively analysed in the context of control methods. This transition is observed for instance over delta wings where the leading edge vortex may suddenly burst at a given axial location, thus engendering a loss of the lift. It can be shown [45] in a linear setting how this situation could be analyzed as a global bifurcation. This bifurcation depends on various factors. First it is related to the local wave stability properties: the flow must be able to transfer energy upstream and downstream. Second the inlet and outlet conditions play a major role in the way these waves are reflected at these boundaries. It is the complete picture that can explain a possible transition threshold. This theoretical investigation emphasizes the role of boundary conditions. It is also shown on a toy problem how, by adding a controller at the inflow boundary, the continuous adjustment of the inlet condition might suppress or at least delay the global bifurcation.

Another interesting aspect of control in fluid dynamics can be found in the paradigm of conducting fluids, where an external magnetic field can be used to drive the fluid through the Lorentz force action. Two similar flows have been investigated. On the one hand, the magnetohydrodynamics mixer [46] consists in forcing a highly viscous conducting fluid in a tank using external inductors. On the other hand, the oscillating buoyant drop [47] corresponds to a liquid sphere with oscillating solid boundaries. In both cases, the advection problem leads to a 1.5 degree-of-freedom Hamiltonian system, which can be conveniently analyzed by means of Melnikov's method. The parameters leading to efficient mixing are analytically determined in the limit of small-amplitude oscillations. For larger amplitudes, global chaos is observed. For example, numerical simulations show that an oscillating drop can be entirely contaminated by species initially located near its periphery.

The surface-tension-driven convection in an electrically conducting liquid layer is another configuration in which an external magnetic field is used to control the flow. The usual control parameter for surface-tension-driven convection is the Marangoni number $Ma = \gamma q^2 H^2/\rho\nu\kappa$, where ρ is the fluid density, H the liquid depth, q the thermal flux, κ the thermal diffusivity and $\gamma = \mathrm{d}\Sigma/\mathrm{d}T$ with Σ the surface tension and T the fluid temperature. In 2D, when no magnetic field is imposed, the first Marangoni instability at Ma_c^1 leads to steady rolls. At $Ma_c^2 > Ma_c^1$ these rolls accelerate, giving rise to an exponential growth of their kinetic energy, a mechanism known as the 'flywheel phenomenon'. In 3D at zero magnetic field, the scenario is different: the first instability yields hexagons that become unstable when Ma is increased. No flywheel effect is observed. Numerically and theoretically, one can study the instability of the 2D rolls towards the 3D hexagonal patterns. The action of an external magnetic field parallel to the initial rolls is first to delay the growth of the instability. Moreover this instability does not result in hexagons but in a chaotic intermittent flow with phases of exponential growth interrupted by roll breakdown and re-organisation [48,49]. When the magnetic field is perpendicular to the liquid layer, the Lorentz force reduces the flywheel phenomenon.

Acknowledgements

We gratefully acknowledge the CNRS (ATIP "Tourbillons en hydrodynamique"), the DGA, the Groupement de Recherche "Turbulence" and the AUM-AFM for financial support.

References

[1] S. Boatto, J. Laskar, Point-vortex cluster formation in the plane and on the sphere: an energy bifurcation condition, Chaos 13 (2003) 824–835.
[2] G.F. Carnevale, J.C. Mc Williams, Y. Pomeau, J.B. Weiss, W.R. Young, Evolution of vortex statistics in two-dimensional turbulence, Phys. Rev. Lett. 66 (1991) 2735–2737.
[3] P. Meunier, U. Ehrenstein, T. Leweke, M. Rossi, A merging criterion for two-dimensional co-rotating vortices, Phys. Fluids 14 (2001) 2757–2766.
[4] C. Josserand, M. Rossi, in preparation.

[5] T. Dubos, A. Babiano, Comparing the two-dimensional cascades of vorticity and passive scalar, J. Fluid Mech. 492 (2003) 131–145.
[6] G. Perret, M. Farge, A. Stegner, A. Azzalini, K. Schneider, Rotating shallow-water flow past an obstacle: numerical and laboratory experiments, in: G.H. Jirka, W.S.J. Uijttewaal (Eds.), Proceeding of the International Symposium on Shallow Flows, vol. II, 16–18 june, 2003, TU Delft, 2003, pp. 61–66.
[7] A. Stegner, T. Pichon, M. Beunier, in press.
[8] G. Rousseaux, H. Yoshikawa, A. Stegner, J.E. Wesfreid, Dynamics of transient vortex above rolling-grain ripples, Phys. Fluids, submitted for publication.
[9] L. Jacquin, D. Fabre, D. Sipp, V. Theofilis, H. Vollmers, Instability and unsteadiness of aircraft wake vortices, Aerospace Sci. Technol. 7 (2003) 577–593.
[10] A. Antkowiak, P. Brancher, Transient energy growth for the Lamb–Oseen vortex, Phys. Rev. Lett. (2003), submitted for publication.
[11] D. Fabre, L. Jacquin, A. Loof, Optimal perturbations in four-vortex aircraft wake in counter-rotating configuration, J. Fluid Mech. 451 (2002) 319–328.
[12] C. Eloy, P. Le Gal, S. Le Dizès, Elliptic and triangular instabilities in rotating cylinders, J. Fluid Mech. 476 (2003) 357–388;
L. Lacaze, P. Le Gal, S. Le Dizes, Elliptical instability in a rotating spheroid J. Fluid Mech., in press.
[13] L. Lacaze, P. Legal, S. Le Dizès, Instabilité elliptique en géométrie sphérique 16^{e}, in : Congrès Français de Mécanique, Nice 1–5 septembre, 2003.
[14] P. Schmid, M. Rossi, Three-dimensional stability of a Burgers vortex, J. Fluid Mech. 500 (2004) 103–112.
[15] Y. Pomeau, Vortex dynamics in perfect fluids, J. Plasma Phys. 56 (1996) 3.
[16] Y. Pomeau, D. Sciamarella, Finite time blowup solutions of 3D incompressible Euler equations: a scenario, J. Fluid Mech. (2003), submitted for publication.
[17] M. Rossi, F. Bottausci, A. Maurel, P. Petitjeans, A non uniformly stretched vortex, Phys. Rev. Lett. 92 (5) (2004) 054504.
[18] Y. Cuypers, A. Maurel, P. Petitjeans, Vortex burst as a source of turbulence, Phys. Rev. Lett. 91 (2003) 194502.
[19] J. Lamoine, A. Maurel, P. Petitjeans, Ph.D. thesis, in preparation.
[20] D. Fabre, L. Jacquin, Viscous instabilities in trailing vortices at large swirl numbers, J. Fluid Mech. 500 (2004) 239–326.
[21] S. Le Dizes, D. Fabre, Asymptotic analysis of viscous centre modes in vortices, in preparation.
[22] I. Delbende, M. Rossi, S. Le Dizès, Stretching effects on the three-dimensional stability of vortices with axial flow, J. Fluid Mech. 454 (2002) 419–442.
[23] L. Jacquin, C. Pantano, On the persistence of trailing vortices, J. Fluid Mech. 471 (2002) 159–168.
[24] P. Billant, J.-M. Chomaz, Experimental evidence for a new instability of a vertical columnar vortex pair in a strongly stratified fluid, J. Fluid Mech. 418 (2000) 167–188.
[25] P. Billant, J.-M. Chomaz, Theoretical analysis of the zigzag instability of a vertical columnar vortex pair in a strongly stratified fluid, J. Fluid Mech. 419 (2000) 29–63.
[26] P. Billant, J.-M. Chomaz, Three-dimensional stability of a vertical columnar vortex pair in a stratified fluid, J. Fluid Mech. 419 (2000) 65–91.
[27] P. Otheguy, P. Billant, J.M. Chomaz, in preparation.
[28] F. Moisy, O. Doaré, O. Daube, T. Pasutto, M. Rabaud, Experimental and numerical study of the shear layer instability between two counter-rotating disks, J. Fluid Mech. 507 (2004) 175–202.
[29] C. Nore, M. Tartar, O. Daube, L.S. Tuckerman, Survey of instability thresholds of flow between exactly counter-rotating disks, J. Fluid Mech. (2004), in press.
[30] C. Nore, L.S. Tuckerman, O. Daube, S. Xin, The 1:2 mode interaction in exactly counter-rotating von Kármán swirling flow, J. Fluid Mech. 477 (2003) 51–88.
[31] T. Gomez, M. Rossi, Instabilité d'une nappe de vorticité étirée instationnaire, C. R. Mecanique 331 (2003) 141–147.
[32] T. Gomez, M. Rossi, Couche de mélange étirée instationnaire : stabilité linéaire, in : 16^{e} Congrès Français de Mécanique, Nice 1–5 septembre, 2003.
[33] L.S. Tuckerman, D. Barkley, Symmetry breaking and chaos in perturbed plane Couette flow, Theoret. Comput. Fluid Dynamics 16 (2002) 91–97.
[34] D. Barkley, L.S. Tuckerman, Stability analysis of perturbed plane Couette flow, Phys. Fluids 11 (1999) 1187–1195.
[35] H. Hristova, S. Roch, P.J. Schmid, L.S. Tuckerman, Transient growth in Taylor–Couette flow, Phys. Fluids 14 (2002) 3475–3484.
[36] M. Abid, A. Verga, Stability of a vortex sheet roll-up, Phys. Fluids 14 (2002) 3829.
[37] G. Pinon, H. Bratec, E. Rivoalen, S. Huberson, Three-dimensionnal jet simulation in cross-flow using vortex method, in: APS DFD 56th Annual Meeting, November 23–25, 2003;
H. Bratec, Modélisation numérique des jets : application aux inverseurs de poussée, Ph.D. Thesis, University of Le Havre (2003) (in French).
[38] S. Julien, J. Lasheras, J.-M. Chomaz, Three-dimensional instability and vorticity patterns in the wake of a flat plate, J. Fluid Mech. 479 (2003) 155–189.
[39] S. Julien, J. Lasheras, J.-M. Chomaz, Secondary instability mechanisms in the wake of a flat plate, in preparation.
[40] L. Schouveiler, A. Brydon, T. Leweke, M.C. Thompson, Interactions of the wakes of two spheres placed side by side, Eur. J. Mech. B Fluids 23 (1) (2004) 137–145.

[41] M.C. Thompson, T. Leweke, A. Cheung, K. Hourigan, Vortex dynamics of particle interactions with walls, in: K. Hourigan, et al. (Eds.), Proceedings of the Conference on Bluff Body Wakes and Vortex-Induced Vibrations, Monash University, Melbourne, Australie, 2002, pp. 113–116, ISBN 0-7326-2108-9.
[42] J.-F. Beaudoin, O. Cadot, J.-L. Aider, E. Weisfreid, Three-dimensional stationary flow over a backward-facing step, Eur. J. Mech. B Fluids (2003), submitted for publication.
[43] M. Marquillie, U. Ehrenstein, On the onset of nonlinear oscillations in a separating boundary-layer flow, J. Fluid Mech. 490 (2003) 169–188.
[44] B. Thiriat, B. Pradal, J.E. Wesfreid, S. Goujon-Durand, Contrôle du sillage d'un cylindre oscillant, in : 16e Congrès Français de Mécanique, Nice 1–5 septembre, 2003.
[45] F. Gallaire, J.-M. Chomaz, P. Huerre, Closed loop control of vortex breakdown: a model study, J. Fluid Mech. (2003), submitted for publication.
[46] J.C. Leprévost, J.R. Angilella, J.P. Brancher, Geometrical analysis of chaotic mixing in a low Reynolds number magnetohydrodynamic quadripolar flow, Phys. Rev. E 63 (2001) 056309.
[47] J.R. Angilella, J.P. Brancher, Note on chaotic advection in an oscillating drop, Phys. Fluids 15 (1) (2003) 261.
[48] T. Boeck, A. Thess, Inertial Bénard–Marangoni convection, J. Fluid Mech. 350 (1997) 149–175.
[49] T. Boeck, A. Thess, Bénard–Marangoni convection at low Prandtl number, J. Fluid Mech. 399 (1999) 251–275.